

Received January 22, 2019, accepted February 8, 2019, date of publication March 28, 2019, date of current version April 24, 2019.

Digital Object Identifier 10.1109/ACCESS.2019.2904531

Compact Microstrip NWB/DWB BPFs With Controllable Isolation Bandwidth for Interference Rejection

XIAO-KUN BI^{ID}, XIAO ZHANG^{ID}, (Member, IEEE),
GUAN-LONG HUANG^{ID}, (Senior Member, IEEE), AND TAO YUAN, (Member, IEEE)

Guangdong Provincial Mobile Terminal Microwave and Millimeter-Wave Antenna Engineering Research Center, College of Information Engineering, Shenzhen University, Shenzhen, Guangdong 518060, China

Corresponding authors: Xiao Zhang (xiao.zhang@szu.edu.cn) and Tao Yuan (yuantao@szu.edu.cn)

This work was supported by the National Natural Science Foundation of China under Grant 61801298 and Grant 61801300.

ABSTRACT In this paper, a novel and planar topology, which can be used to design notched-/dual-wideband bandpass filters (NWB/DWB BPFs) with controllable isolation bandwidth, is presented for interference rejection. Here, the isolation band is referred to notch band for NWB BPFs, while stopband between two passbands for DWB BPFs. The proposed topology is started from a novel T-shaped resonator with two poles and three zeros. Then, a pair of parallel-coupled lines and two open-ended stubs is added. With the help of the added parts, the extra four poles are introduced, and another two zeros are suppressed or excited according to whether it is required to realize a notched- or dual-band response. Due to the existence of multiple transmission poles and zeros, the excellent filtering responses, i.e., high isolation level, sharp selectivity, and good passband flatness, can be achieved. Besides, it is found that the isolation bandwidth of BPFs based on the proposed topology can be continuously varied from a narrow notch band to a wide stopband while the outer two passband edges are maintained unchanged by using suitable parameters. To validate this, two prototypes are designed and measured, including a six-mode NWB BPF with 3-dB passband fractional bandwidth (FBW) of 94.1% and 20-dB notch FBW of 2.39%, and a three-mode DWB BPF with 3-dB passband FBWs of 36.2% and 22.6% and 20-dB stopband FBW of 14.5%.

INDEX TERMS Controllable isolation bandwidth, interference rejection, multiple transmission poles and zeros, notched-/dual-wideband bandpass filters, T-shaped resonator.

I. INTRODUCTION

Due to the desirable features, such as, low profile, compact size, low cost, and easy integration with other components, the microstrip filters are extensively used in the modern wire-less communication systems. To satisfy various requirements, the microstrip filters with different performances have been designed, including low-pass filters [1], [2], stopband filters [3], [4], single-/multi-band BPFs [5], [6], reconfigurable BPFs [7], [9], balanced BPFs [10], [11], and high-pass filters [12].

In a high data-rate telecommunication system, the microstrip notched-/dual-wideband bandpass filters (NWB/DWB BPFs) with good filtering responses and compact size play

a very important role. Until now, different topologies and design methods have been proposed for the designs of NWB BPFs [13], [14] and DWB BPFs [15]–[18]. Although the desired notched-/dual-wideband filtering responses could be achieved in the previous works, it is still a great challenge to design a NWB BPF and DWB BPF simultaneously by using a common topology, especially for the ones with controllable isolation bandwidth and fixed outer passband edges, which can be used to prevent the telecommunication systems from interference more precisely and effectively.

In this paper, a novel and simple planar topology, which can be used to design both NWB BPFs and DWB BPFs simultaneously, is presented for interference rejection. The proposed topology is based on a novel T-shaped resonator, which owns two poles and three zeros. To incorporate this T-shaped resonator for the desired filters, two

The associate editor coordinating the review of this manuscript and approving it for publication was Lin Peng.

open-ended stubs and a pair of symmetrical PCLs are introduced. The notched-/dual-band response is determined by the electrical length of the open-ended stubs. By using the even-/odd-mode analysis method and S -parameters theory, trans-mission poles (TPs) and transmission zeros (TZs) can be theoretically extracted. Besides, it is found that the isolation bandwidth of BPFs based on the proposed topology can be varied from a narrow notch band to a wide stopband with the help of the suitable parameters, while the outer two passband edges are kept fixed. To the best knowledge of authors, the BPFs with controllable isolation bandwidth and fixed outer passband edges have never been reported before.

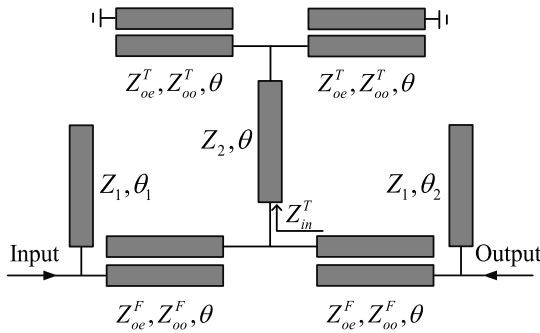


FIGURE 1. The circuit schematic of the proposed filters.

II. BASIC THEORY

As shown in Fig. 1, the circuit schematic of proposed filters, for both NWB/DWB BPF integration, is formed by a single T-shaped resonator with a pair of symmetrical PCLs and two open-ended stubs. The T-shaped resonator is constructed by a connected transmission line and other pair of symmetrical PCLs, whose electrical length is θ ($\theta = \pi/2$ at the operating frequency f_0) and characteristic impedance are Z_2, Z_{oe}^T, Z_{oo}^T . Thus, the input impedance of this T-shaped resonator can be written as:

$$Z_{in}^T = jZ_2 \frac{(A_T^2 - B_T^2) - (B_T^2 + 4A_T Z_0) \tan^2 \theta}{[B_T^2 \tan^2 \theta - (4A_T Z_0 + A_T^2 - B_T^2)] \tan \theta} \quad (1a)$$

with

$$A_T = Z_{oe}^T + Z_{oo}^T \quad (1b)$$

$$B_T = Z_{oe}^T - Z_{oo}^T \quad (1c)$$

According to (1), two poles f_{p1}^T, f_{p2}^T and three zeros $f_{z1}^T, f_{z2}^T, f_{z3}^T$ can be found, as shown in Fig. 2. For arbitrary Z_{oe}^T, Z_{oo}^T , and Z_2 , the relationship of $f_{z1}^T < f_{p1}^T < f_{z2}^T = f_0 < f_{p2}^T < f_{z3}^T$ holds. To incorporate this T-shaped resonator for the desired filters with excellent filtering responses, extra poles and zeros should be introduced. Therefore, a pair of PCLs with $\theta, Z_{oe}^F, Z_{oo}^F$ and two open-ended stubs with θ_1, θ_2, Z_1 are added.

A. NWB BPFs WITH CONTROLLABLE NOTCH-BAND BANDWIDTH

When $\theta_1 = \theta_2 = \theta$, the proposed topology can be used to de-sign NWB BPFs with a notch band. Due to the symmetry,

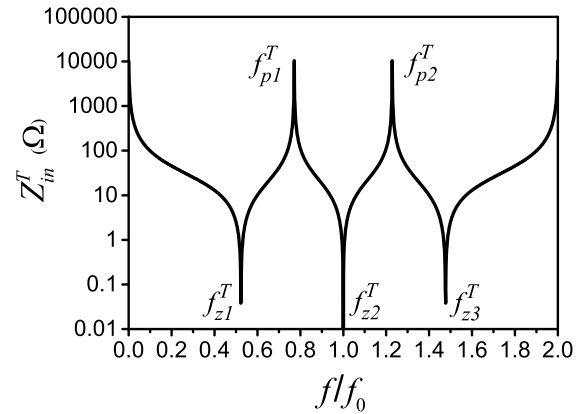


FIGURE 2. The input impedance of the novel T-shaped resonator.

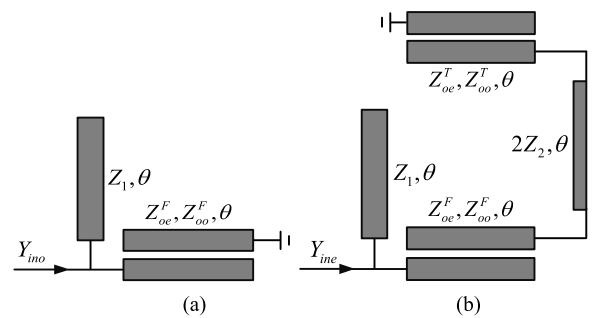


FIGURE 3. (a) Odd- and (b) even-mode equivalent circuits of the proposed NWB BPFs.

the TPs can be determined by using the even-/odd-mode analysis method. The odd-/even-mode equivalent circuits are shown in Fig. 3. For the odd-mode equivalent circuit shown in Fig. 3(a), the input admittance Y_{ino} can be obtained as

$$Y_{ino} = j \frac{1}{Z_1} \tan \theta + \frac{2jA_F \tan \theta}{A_F^2 - B_F^2 - B_F^2 \tan^2 \theta} \quad (2a)$$

where

$$A_F = Z_{oe}^F + Z_{oo}^F \quad (2b)$$

$$B_F = Z_{oe}^F - Z_{oo}^F \quad (2c)$$

When the resonance condition $Y_{ino} = 0$ is considered, the odd-mode resonance frequencies can be determined as

$$f_{op1} = f_0 - \frac{2f_0}{\pi} \arctan \left(\sqrt{\frac{A_F^2 - B_F^2 + 2A_F Z_1}{B_F^2}} \right) \quad (3a)$$

$$f_{op2} = f_0 + \frac{2f_0}{\pi} \arctan \left(\sqrt{\frac{A_F^2 - B_F^2 + 2A_F Z_1}{B_F^2}} \right) \quad (3b)$$

For the even-mode equivalent circuit shown in Fig. 3(b), its input admittance Y_{ine} can be written as

$$Y_{ine} = j \frac{1}{Z_1} \tan \theta + \frac{2A_F \tan \theta + 8jZ_{in}^T \tan^2 \theta}{4A_F Z_{in}^T \tan \theta + j(B_F^2 \tan^2 \theta + B_F^2 - A_F^2)} \quad (4)$$

When $Y_{ino} = 0$, another four resonant frequencies can be determined and expressed as

$$f_{ep1} = f_0 - \frac{2f_0}{\pi} \arctan \left(\sqrt{\frac{\Delta_2 + \sqrt{\Delta_2^2 - 4\Delta_1\Delta_3}}{2\Delta_1}} \right) \quad (5a)$$

$$f_{ep2} = f_0 - \frac{2f_0}{\pi} \arctan \left(\sqrt{\frac{\Delta_2 - \sqrt{\Delta_2^2 - 4\Delta_1\Delta_3}}{2\Delta_1}} \right) \quad (5b)$$

$$f_{ep3} = f_0 + \frac{2f_0}{\pi} \arctan \left(\sqrt{\frac{\Delta_2 - \sqrt{\Delta_2^2 - 4\Delta_1\Delta_3}}{2\Delta_1}} \right) \quad (5c)$$

$$f_{ep4} = f_0 + \frac{2f_0}{\pi} \arctan \left(\sqrt{\frac{\Delta_2 + \sqrt{\Delta_2^2 - 4\Delta_1\Delta_3}}{2\Delta_1}} \right) \quad (5d)$$

where

$$\Delta_1 = B_F^2 B_T^2 \quad (6a)$$

$$\Delta_2 = 4Z_2(A_F + 2Z_1)(B_T^2 + 4A_T Z_2) + B_T^2(A_F^2 - B_F^2) + B_F^2(2A_F Z_1 + 4A_T Z_2 + A_T^2 - B_T^2) \quad (6b)$$

$$\Delta_3 = (4A_T Z_2 + A_T^2 - B_T^2)(2A_F Z_1 + A_F^2 - B_F^2) + 4Z_2(A_F + 2Z_1)(A_T^2 - B_T^2) \quad (6c)$$

By introducing a pair of TZs near the passband edges, a sharp rejection response can be realized. Considering Fig. 3(a) and (b), the transmission coefficient S_{21} can be expressed as

$$S_{21} = \frac{Y_0(Y_{ine} - Y_{ino})}{(Y_0 + Y_{ine})(Y_0 + Y_{ino})} \quad (7)$$

Hence, the TZs can be determined when $Y_{ine} = Y_{ino}$. After some algebraic operations, the TZs can be written as

$$f_{z1} = \frac{2f_0}{\pi} \arctan \left(\sqrt{\frac{A_T^2 - B_T^2}{4A_T Z_2 + B_T^2}} \right) \quad (8a)$$

$$f_{z2} = f_0 \quad (8b)$$

$$f_{z3} = 2f_0 - \frac{2f_0}{\pi} \arctan \left(\sqrt{\frac{A_T^2 - B_T^2}{4A_T Z_2 + B_T^2}} \right) \quad (8c)$$

Based on the above theoretical analysis, it is obviously that the NWB BPFs based on the proposed topology own six TPs and three TZs, which are all symmetrical with respect to f_0 . The TZs are all from the T-shaped resonator, which can be directly used for the implementation of a notch band and sharp passband selectivity. The odd-mode TPs are all created from the added parts, while the even-mode TPs are created from the added parts and novel T-shaped resonator together. All the TPs can be used for good passband flatness. For arbitrary $Z_1, Z_{oe}^F, Z_{oo}^F, Z_2, Z_{oe}^T$ and Z_{oo}^T , the relationship

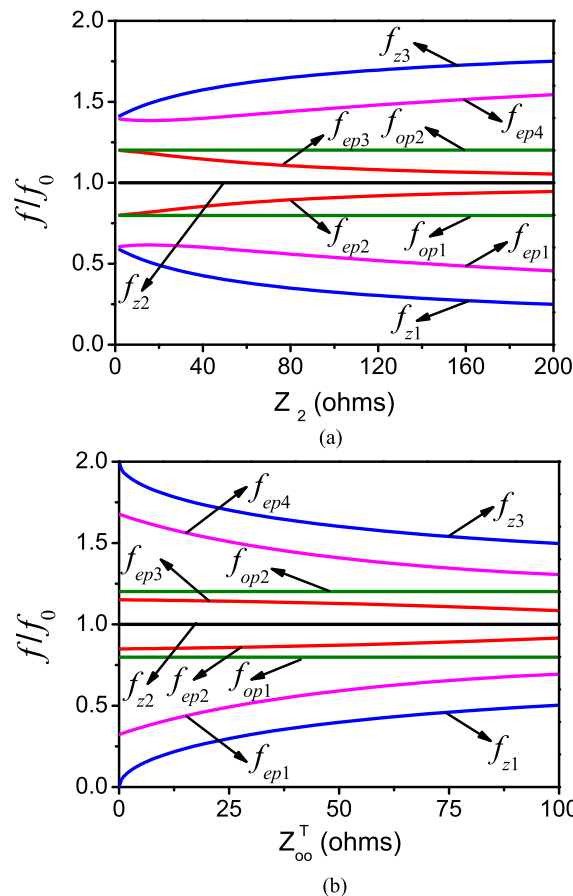


FIGURE 4. TPs and TZs of the proposed topology for NWB BPFs respect to different (a) $Z_2 (Z_{oo}^T = 46.9 \Omega)$; (b) $Z_{oo}^T (Z_2 = 41.2 \Omega)$. Other parameters are recorded as: $Z_1 = 250 \Omega, Z_{oo}^F = 39.1 \Omega, Z_{oe}^F = 171 \Omega, Z_{oe}^T = 179 \Omega$.

of $f_{z1} < f_{ep1} < f_{op1} < f_{ep2} < f_{z2} = f_0 < f_{ep3} < f_{op2} < f_{ep4} < f_{z3}$ holds. Therefore, the notch bandwidth is mainly controlled by the locations of f_{ep2} and f_{ep3} , while the passband bandwidth of NWB BPF is mainly controlled by the ones of f_{ep1} and f_{ep4} .

To better understand the design mechanism, the effects of T-shaped resonator's parameters Z_2, Z_{oo}^T and Z_{oo}^T on TPs/TZs are studied, as illustrated in Fig. 4. Seen from Fig. 4(a), f_{z1} and f_{z2} will move apart while f_{ep2} and f_{ep3} are closer when the parameter Z_2 increases. Meanwhile, the TPs f_{ep1} and f_{ep4} are less affected by the parameter Z_2 . When the parameter Z_{oo}^T is fixed, the TZs f_{z1}, f_{z2} and TPs f_{ep1}, f_{ep4} will move closer to each other with the increase of Z_{oo}^T , while f_{ep2} and f_{ep3} are rarely changed, as shown in Fig. 4(b). Therefore, the notch bandwidth can be tuned by altering the value of Z_2 , while the filter bandwidth can be tuned by altering Z_{oo}^T and Z_{oe}^T . When Z_2, Z_{oo}^T and Z_{oe}^T are only altered to control the notch and filter bandwidths, the filtering response degrades. Adjusting Z_1, Z_{oe}^F, Z_{oo}^F can improve the performance. The minimum dimension realized on the substrate used in this paper and range on characteristic impedance are set as 0.1 mm and 5 – 250 Ω respectively. Two frequency-response examples with good in- and out-of-band responses for wide

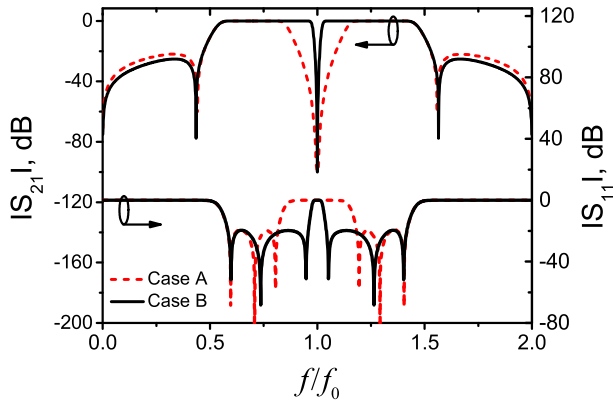


FIGURE 5. Two calculated frequency responses for the proposed NWB BPFs with a narrowband (Case A) and wideband (Case B) notch.

and narrow notch bands are shown in Fig. 5. Accordingly, one can easily understand that the notch bandwidth can be continuously changed from narrow to wide while passband bandwidth is fixed.

B. DWB BPFs WITH CONTROLLABLE STOPBAND BANDWIDTH

As shown in Fig. 5, the selectivity of the proposed NWB BPF near the notch band is very poor when the notch band-width is wide. To improve this, the effects of θ_1 and θ_2 on the filters' performance are studied here.

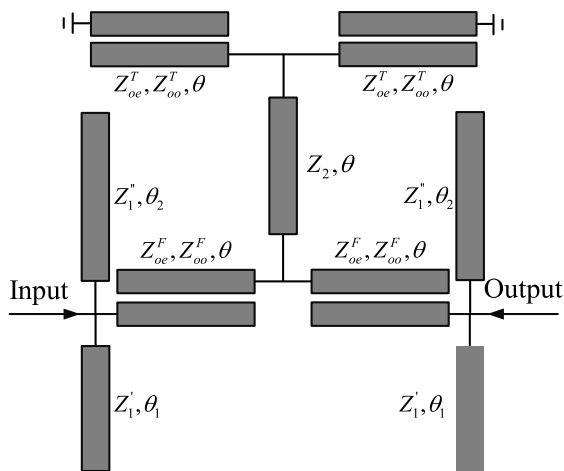


FIGURE 6. The modified circuit schematic of the DWB BPFs for the theoretical analysis ($Z_1' = Z_1'' = 2Z_1$).

To better analyze this structure, the two open-ended stubs are theoretically replaced by two pairs of symmetrical stubs with Z_1', θ_1 and Z_1'', θ_2 respectively, as shown in Fig. 6. Then, $\Delta\theta = 1.2(\theta - \theta_1) = \theta_2 - \theta$. When $\Delta\theta = 0$, the proposed topology can be used to design NWB BPFs with a wide notch bandwidth, as mentioned in Part A. Increasing $\Delta\theta$, another two additional zeros f_{11} and f_{12} are introduced and move apart, while the TPs f_{ep2}, f_{ep3} slightly depart. For the rest poles and zeros, they are kept

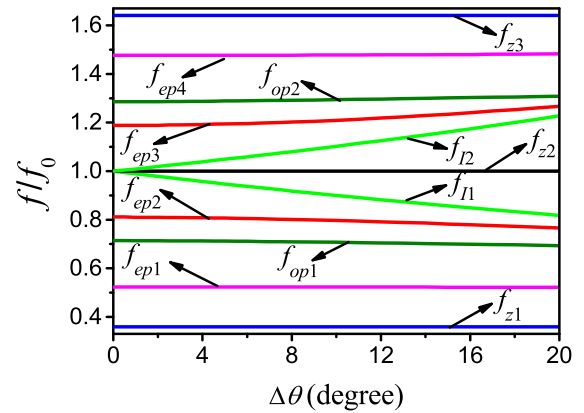


FIGURE 7. TPs and TZs of the proposed topology versus different $\Delta\theta$ ($Z_1' = Z_1'' = 334 \Omega, Z_2 = 57.4 \Omega, Z_{oe}^F = 175 \Omega, Z_{oo}^F = 30.4 \Omega, Z_{oe}^T = 167.5 \Omega, Z_{oo}^T = 29.8 \Omega$).

unaltered, as shown in Fig. 7. The original NWB BPF with a notch band is changed to be a DWB BPF with stopband between two passbands. Thus, the selectivity near the notch band can be effectively improved by altering the electrical length θ_1 and θ_2 . The relationship among electrical length θ_1 , θ_2 and TZs f_{11}, f_{12} are written as

$$f_{11} = \frac{\pi}{2\theta_2} f_0 \tag{9a}$$

$$f_{12} = \frac{\pi}{2\theta_1} f_0 \tag{9b}$$

For smaller θ_1 (larger θ_2), the lower (upper) pass-band edge of second (first) passband will move upwards (downwards), while the other three ones are maintained unchanged. Besides, the flatness in the passbands and isolation level in the stop-band deteriorate, as illustrated in Fig. 8. Therefore, the filter's stopband bandwidth can be independently controlled by θ_1 and θ_2 . Furthermore, three indicators, including the flatness in the passbands, selectivity near the stopband, and isolation in the stopband, should be considered simultaneously when determining the electrical length θ_1 and θ_2 .

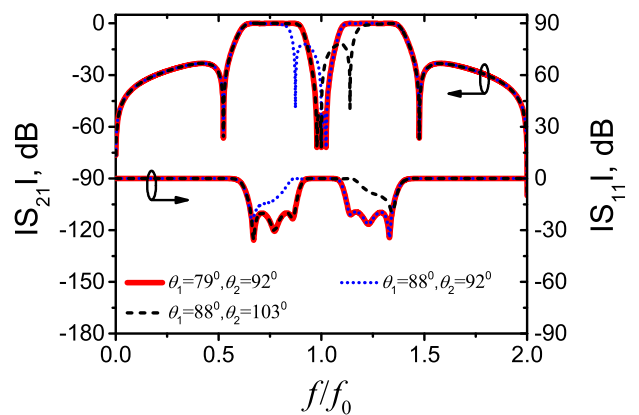


FIGURE 8. Three calculated frequency responses for the proposed DWB BPF with different electrical length of θ_1 and θ_2 .

III. DESIGN PROCEDURE & EXAMPLES OF SWB BPF AND DWB BPF

A. DESIGN PROCEDURE

Based on the theoretical analysis mentioned above, a simple design procedure can be summarized as:

1) Given the requirements of the desired filter, i.e., the desired operating frequency (f_0), isolation bandwidth, return loss(es) in the passband(s), passband bandwidth(s), selectivity in the transition bands, center frequency ratio (CFR), and isolation in the stopband. The last two indicators are only for the DWB BPFs.

2) When the value of Z_2 is large, the proposed topology is suitable to design NWB BPFs with a narrow notch. The parameters $Z_1, Z_{oe}^F, Z_{oo}^F, Z_{oe}^T$ and Z_{oo}^T can be used to optimize the passband bandwidth, selectivity in the transition bands, and return loss in the passband.

3) When the value of Z_2 is small, the proposed topology is suitable to design DWB BPFs with a wide stopband. The parameters $Z_1, Z_{oe}^F, Z_{oo}^F, Z_{oe}^T, Z_{oo}^T, \theta_1$ and θ_2 can be used to optimize the passband bandwidths, return losses in the pass-bands, selectivity in the transition bands, isolation in the stopband, CFR, and stopband bandwidth.

4) For further optimization, slightly adjust of the values of $Z_1, Z_2, Z_{oe}^F, Z_{oo}^F, Z_{oe}^T, Z_{oo}^T, \theta_1$ and θ_2 (θ_1 and θ_2 are only for the DWB BPFs) to achieve the desired performances.

In terms of the optimized parameters, the layouts of de-sired filters can be determined with the help of commercial software tools. Two design skills are used in the layouts: 1) To enhance the coupling strength of feedlines, hboxed the open-ended stubs are parallel with PCLs with Z_{oe}^F and Z_{oo}^F . 2) As the effects of open-ended stubs on the filter response will reduce with the shorter separation between the stubs and PCLs with Z_{oe}^F and Z_{oo}^F , the stubs and PCLs are replaced by a pair of parallel-coupled three-lines when the value of Z_1 is much larger than 250Ω . This one is only suitable to the de-sign of NWB BPFs.

B. FILTER I

According to above design procedure, the circuit parameters of a NWB BPF (Filter I) with 3-dB FBW 92.8%, 20-dB notch FBW 2.3%, and center frequency at 4.5 GHz, are selected as: $\theta = 90^\circ, Z_1 = 1300\Omega, Z_2 = 45.8\Omega, Z_{oe}^F = 138\Omega, Z_{oo}^F = 37.3 \Omega, Z_{oe}^T = 97.2 \Omega,$ and $Z_{oo}^T = 49.7 \Omega$. The simulated S -parameters of the ideal circuit are shown in Fig. 4 (Case B). As the substrate used in this work is Rogers RO4003B with $\epsilon_r = 3.38$ and $h = 0.813$ mm, the dimensions and layout of proposed NWB BPF can be determined with the help of full-wave electromagnetic solver, as shown in Fig. 9. The overall circuit size is $31.0 \text{ mm} \times 18.0 \text{ mm}$ ($0.86 \lambda_g \times 0.49 \lambda_g$, where λ_g is the guided wavelength of the $50\text{-}\Omega$ microstrip line on the used substrate at the center frequency f_0).

The simulated and measured results are shown in Fig. 10(a).

It is apparently the measured results are in good agreement with the simulated ones. The measured passband range is

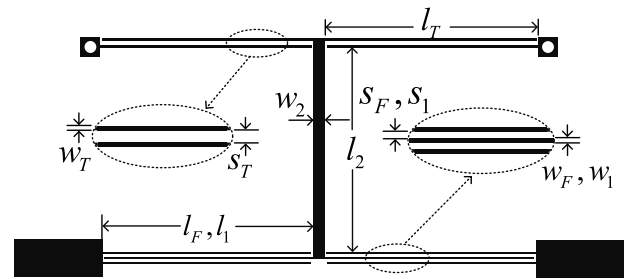
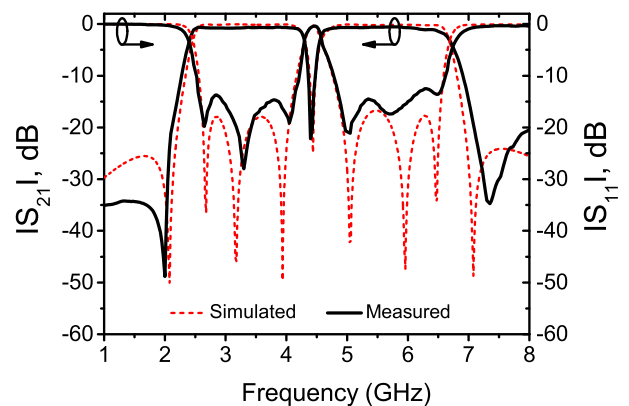


FIGURE 9. The layout of the designed NWB BPF (unit: mm, $s_1 = s_F = 0.14, l_1 = l_F = 10.6, w_1 = w_F = 0.1, l_2 = 10.3, w_2 w_2 = 0.6, s_T = 0.27, l_T = 10.7, w_T = 0.1$).



(a)



(b)

FIGURE 10. a) The simulated and measured S -parameters, and b) photograph of NWB BPF with controllable notch bandwidth.

from 2.41 to 6.69 GHz with a FBW of 94.1%. Six TPs are found at 2.65, 3.23, 4.05, 5.05, 5.75, and 6.47 GHz. The measured minimum insertion loss (IL) is 0.42 dB in the passband. For the notch band, it is located at 4.45 GHz. The 20-dB notch FBW is 2.39%. Besides, the attenuation slopes in the lower and upper transition bands are 113 and 49 dB/GHz respectively, with two zeros at 2.01 GHz and 7.35 GHz. The measured group delay is as good as 0.75 ns. In Fig. 9(b), the photograph of the fabricated NWB BPF is given.

To highlight the advantages of this filter, a comparison with the reported works is listed in Table 1. It is apparently that the proposed design is featured as a controllable notch bandwidth.

C. FILTER II

For the wide stopband bandwidth design, the circuit parameters of the proposed DWB BPF (Filter II) are selected as: $\theta = 90^\circ, \theta_1 = 88^\circ, \theta_2 = 92^\circ, Z_1 = 300\Omega,$

TABLE 1. Comparison with previous works.

	f_0 (GHz)	TPs/TZs	3-dB FBW	Notch	Group delay (ns)	IL ¹ (dB)	NBC ²
[13]	6.65	4/4	94.7%	1	< 0.5	0.45	no
[14]	6.85	4/2	109%	1	< 0.27	0.9	no
Filter I	4.55	6/3	94.1%	1	< 0.75	0.42	yes

IL¹: The insertion loss in the passband; NBC²: notch band controllability.

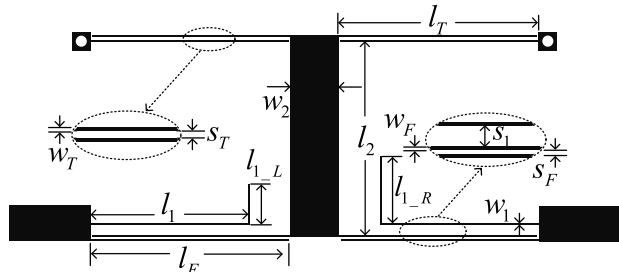


FIGURE 11. The layout of the designed DWB BPF (unit: mm, $s_F = 0.1$, $l_F = 10.8$, $w_F = 0.1$, $s_1 = 0.56$, $l_1 = 8.5$, $w_1 = 0.1$, $l_{1L} = 2.1$, $l_{1R} = 3.6$, $l_2 = 10.44$, $w_2 = 2.6$, $s_T = 0.16$, $l_T = 10.7$, $w_T = 0.1$).

$Z_2 = 26 \Omega$, $Z_{oe}^F = 136\Omega$, $Z_{oo}^F = 37.5\Omega$, $Z_{oe}^T = 145\Omega$, $Z_{oo}^T = 57.5\Omega$, and $f_0 = 4.5$ GHz. The simulated results of the ideal circuit are shown in Fig. 8 (solid line). The proposed filter is manufactured on the substrate of Rogers RO4003B with $\epsilon_r = 3.38$ and $h = 0.813$ mm. The final layout and dimensions of Filter II, as shown in Fig. 11, can be determined with the help of full-wave electro-magnetic solver. The filter is symmetrical except that l_{1L} is not equals to l_{1R} . The overall circuit size is 33.0 mm * 16.0 mm ($0.69 \lambda_g * 0.34 \lambda_g$, where λ_g is the guided wavelength of the 50- Ω microstrip line on the substrate at the center frequency of the first passband).

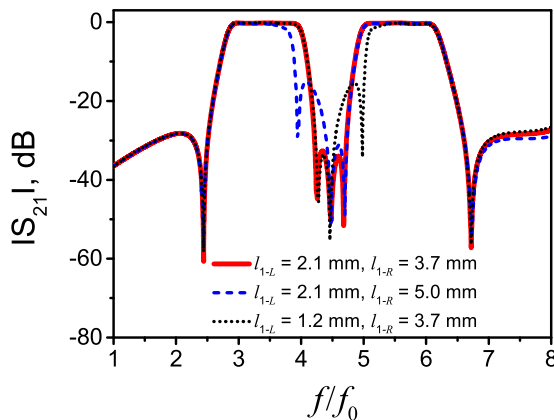


FIGURE 12. The simulated results of layout with different l_{1L} and l_{1R} .

For the simulated results of layout with different l_{1L} and l_{1R} , they are shown in Fig. 12. Obviously, the upper passband edge of first passband is independently controlled by the physical length l_{1R} , while the lower passband edge of second

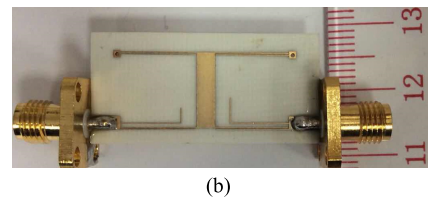
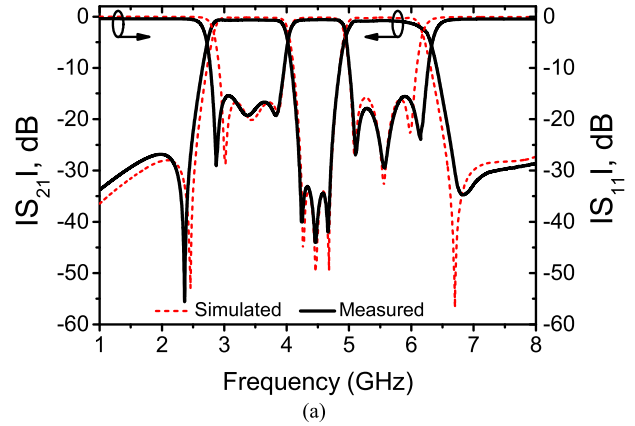


FIGURE 13. (a) The simulated and measured S-parameters, and (b) photograph of DWB BPF with controllable stopband bandwidth.

TABLE 2. Comparison with previous works.

	f_0 (GHz)	TPs/TZs	3-dB FBWs (%)	RL in the passband (dB)	IL in the stopband (dB)	Group delay (ns)	SBC ¹
[9]	3.66/6.05	6/7	20.8/17.3	13/15	20	< 1.7	no
[15]	0.705/1.37	6/8	41.1/19.0	13/15	19	< 7.45	no
[16]	1.92/5.44	5/3	66.7/28.3	15/17	25	N/A	no
[17]	2.3/5.25	3/2	54/20	10/10	20	< 1.8	no
Filter II	3.38/5.62	6/5	36.2/22.6	13/14	25	< 2.4	yes

SBC¹: stopband controllability.

passband is independently controlled by the physical length l_{1L} . Thus, the bandwidth of stopband between two passbands can be fully controlled in continuous manners while the outer two passband edges are kept fixed.

The simulated and measured results are compared in Fig. 13(a). Seen from it, the measured and simulated results are in good agreement with each other. The measured two pass-band 3-dB fractional bandwidths are 36.2% and 22.6% with respect to the center frequencies of 3.38 and 5.62 GHz, respectively. At the center frequencies, the measured ILs are 0.49 dB for the first passband and 0.65 dB for the second one. The return loss (RL) is better than 13.0 dB from 2.78 to 3.89 GHz in the first passband and better than 14.0 dB from 5.07 to 6.19 GHz in the second passband. Besides, a wide stopband over 20-dB isolation is achieved from 4.15 to 4.80 GHz, indicating high isolation level between two passbands. With reference to the operating frequency $f_0 = 4.5$ GHz, the 20-dB stopband FBW is 14.5%.

In the first passband, there are three measured TPs found at 2.87, 3.38, and 3.81 GHz; in the second passband, other three measured TPs are located at 5.14, 5.6, and 6.12 GHz. For the measured TZs, they are located at 2.36, 4.26, 4.48, 4.69, and 6.82 GHz respectively. The attenuation slopes in the four transition bands are 130, 161, 145, and 59.7 dB/GHz respectively. The group delay varies from 0.5 to 1.6 ns for first passband and 0.7 to 2.4 ns for second passband. In Fig. 11(b), the photograph of DWB BPF is displayed.

To highlight the advantages of the proposed DWB BPF, a comparison with some previous works is also listed in Table 2. Obviously, the proposed design is featured as the controllable bandwidth of stopband between two passbands.

IV. CONCLUSION

In this paper, a novel and planar topology is presented for the designs of NWB/DWB BPFs with controllable isolation bandwidth. The proposed topology is constructed by a novel T-shaped resonator with two open-ended stubs and a pair of PCLs. The notched-/dual-band response is realized by controlling the electrical length of open-ended stubs. For the six-mode NWB BPF, there is a narrow notch band found in the measured results; for the three-mode DWB BPF, there is a wide stopband found in the measured results. The measured results demonstrate the validity of the proposed topology and method. The filters based on the proposed topology exhibit some merits, i.e., controllable isolation bandwidth, compact size, excellent filtering responses, and easy implementation. It is anticipated that this topology could be extensively used in the multi-standard wireless systems.

REFERENCES

- [1] S. Luo, L. Zhu, and S. Sun, "Stopband-expanded low-pass filters using microstrip coupled-line hairpin units," *IEEE Microw. Wireless Compon. Lett.*, vol. 18, no. 8, pp. 506–508, Aug. 2008.
- [2] Q. He and C. Liu, "A novel low-pass filter with an embedded band-stop structure for improved stop-band characteristics," *IEEE Microw. Wireless Compon. Lett.*, vol. 19, no. 10, pp. 629–631, Oct. 2009.
- [3] K. Rambabu, M. Y.-W. Chia, K. M. Chan, and J. Bornemann, "Design of multiple-stopband filters for interference suppression in UWB applications," *IEEE Trans. Microw. Theory Techn.*, vol. 54, no. 8, pp. 3333–3338, Aug. 2006.
- [4] N. Jankovic, R. Geschke, and V. Crnojevic-Bengin, "Compact tri-band bandpass and bandstop filters based on Hilbert-fork resonators," *IEEE Microw. Wireless Compon. Lett.*, vol. 23, no. 6, pp. 282–284, Jun. 2013.
- [5] C.-J. Chen, "Design of parallel-coupled dual-mode resonator bandpass filter," *IEEE Trans. Compon., Packag. Manuf. Technol.*, vol. 6, no. 10, pp. 1542–1548, Oct. 2016.
- [6] F. Song, B. Wei, L. Zhu, Y. Feng, R. Wang, and B. Cao, "A novel tri-band superconducting filter using embedded stub-loaded resonators," *IEEE Trans. Appl. Supercond.*, vol. 26, no. 8, Dec. 2016, Art. no. 1502009.
- [7] C.-W. Tang, C.-T. Tseng, and S.-C. Chang, "Design of the compact tunable filter with modified coupled lines," *IEEE Trans. Compon., Packag. Manuf. Technol.*, vol. 4, no. 11, pp. 1815–1821, Nov. 2014.
- [8] H.-Y. Tsai, T.-Y. Huang, and R.-B. Wu, "Varactor-tuned compact dual-mode tunable filter with constant passband characteristics," *IEEE Trans. Compon., Packag. Manuf. Technol.*, vol. 6, no. 9, pp. 1399–1407, Sep. 2016.
- [9] X.-K. Bi, T. Cheng, P. Cheong, S.-K. Ho, and K.-W. Tam, "Design of dual-band bandpass filters with fixed and reconfigurable bandwidths based on terminated cross-shaped resonators," *IEEE Trans. Circuits Syst. II, Exp. Briefs*, vol. 66, no. 3, pp. 317–321, Mar. 2019. doi: 10.1109/TCSII.2018.2848667.
- [10] Y. Wu, L. Cui, W. Zhang, L. Jiao, Z. Zhuang, and Y. Liu, "High performance single-ended wideband and balanced bandpass filters loaded with stepped-impedance stubs," *IEEE Access*, vol. 5, pp. 5972–5981, 2017.
- [11] J.-X. Chen, M.-Z. Du, Y.-L. Li, Y.-J. Yang, and J. Shi, "Independently tunable/controllable differential dual-band bandpass filters using element-loaded stepped-impedance resonators," *IEEE Trans. Compon., Packag. Manuf. Technol.*, vol. 8, no. 1, pp. 113–120, Jan. 2018.
- [12] J. Ni and J.-S. Hong, "Compact varactor-tuned microstrip high-pass filter with a quasi-elliptic function response," *IEEE Trans. Microw. Theory Techn.*, vol. 61, no. 11, pp. 3853–3859, Nov. 2013.
- [13] H. Wang, K.-W. Tam, S.-K. Ho, W. Kang, and W. Wu, "Design of ultra-wideband bandpass filters with fixed and reconfigurable notch bands using terminated cross-shaped resonators," *IEEE Trans. Microw. Theory Techn.*, vol. 62, no. 2, pp. 252–265, Feb. 2014.
- [14] Y. Mondal and Y. L. Guan, "A coplanar stripline ultra-wideband bandpass filter with notch band," *IEEE Microw. Wireless Compon. Lett.*, vol. 20, no. 1, pp. 22–24, Jan. 2010.
- [15] Y. Wu, L. Cui, Z. Zhuang, W. Wang, and Y. Liu, "A simple planar dual-band bandpass filter with multiple transmission poles and zeros," *IEEE Trans. Circuits Syst. II, Exp. Briefs*, vol. 65, no. 1, pp. 56–60, Jan. 2018.
- [16] J. Xu, Y.-X. Ji, C. Miao, and W. Wu, "Compact single-/dual-wideband BPF using stubs loaded SIR (SsLSIR)," *IEEE Microw. Wireless Compon. Lett.*, vol. 23, no. 7, pp. 338–340, Jul. 2013.
- [17] C.-W. Tang and Y. K. Hsu, "Design of wide-single-/dual-passband bandpass filters with comb-loaded resonators," *IET Microw. Antennas Propag.*, vol. 6, no. 1, pp. 10–16, Jan. 2012.
- [18] K.-S. Chin and J.-H. Yeh, "Dual-wideband bandpass filter using short-circuited stepped-impedance resonators," *IEEE Microw. Wireless Compon. Lett.*, vol. 19, no. 3, pp. 155–157, Mar. 2009.



XIAO-KUN BI was born in Henan, China, in 1987. He received the B.Sc. degree in electrical & information engineering from the North University of China, Taiyuan, China, in 2010, the M.Sc. degree in signal and information processing from Nankai University, Tianjin, China, in 2015, and the Ph.D. degree in electrical and computer engineering from the University of Macau, Macau, in 2019.

Since 2014, he has been a Research Assistant with the University of Macau. His research interests include notched-/dual-wideband bandpass filters, reconfigurable filters, slotline antennas, and their applications in modern communication systems.



XIAO ZHANG (S'15–M'18) was born in Gaozhou, China. He received the B.Eng. degree in information engineering and the M.Eng. degree in communication and information systems from the South China University of Technology, Guangzhou, China, in 2011 and 2014, respectively, and the Ph.D. degree in electrical and computer engineering from the University of Macau, Macau, China, in 2017.

From 2012 to 2014, he was a Research Assistant with Comba Telecom Systems Limited, Guangzhou, China. He joined the Antenna and Electromagnetic-Wave Laboratory, University of Macau, as a Research Fellow, in 2018. He is currently an Assistant Professor with the College of Information Engineering, Shenzhen University, Shenzhen, China. His research interests include planar antennas and microwave circuits.



GUAN-LONG HUANG (M'11–SM'18) received the B.E. degree in electronic information engineering from the Harbin Institute of Technology, Harbin, China, and the Ph.D. degree in electrical and computer engineering with the National University of Singapore, Singapore.

He has been with Temasek Laboratories, National University of Singapore, as a Research Scientist, and Nokia Solutions and Networks System Technology as a Senior Antenna Specialist from 2011 to 2017. He is currently an Assistant Professor with the College of Information Engineering, Shenzhen University, Shenzhen, Guangdong, China. He also serves as the Deputy Director for the Guangdong Provincial Mobile Terminal Micro-wave and Millimeter-Wave Antenna Engineering Research Center. He has authored or co-authored more than 100 papers in journals and conferences. His research interests include design and implementation of planar antenna arrays, 5G base-station and mobile RF front-end devices/antennas, phased antenna arrays, channel coding for massive MIMO applications, and 3-D printing technology in microwave applications. He is currently serving as an Associate Editor for the journal IEEE Access.



TAO YUAN received the bachelor's and master's degrees from Xidian University, China, and the Ph.D. degree from the National University of Singapore, Singapore. He is currently a Professor with the College of Information Engineering, Shenzhen University, Shenzhen, China. His current research interests include developing novel RF modules, and antennas for mobile terminal and 5G applications.

...